

# Snow and Water Imaging Spectrometer (SWIS): optomechanical and system design for a CubeSat-compatible instrument

Holly A. Bender\*, Pantazis Mouroulis, Christopher D. Smith<sup>a</sup>, Colin H. Smith, Byron E. Van Gorp,  
Michael L. Eastwood, Johannes Gross  
Jet Propulsion Laboratory, California Institute of Technology, Pasadena, California, USA  
<sup>a</sup>ATK Space Systems Inc., Pasadena, California, USA

## ABSTRACT

The Snow and Water Imaging Spectrometer (SWIS) is a fast, high-uniformity, low-polarization sensitivity imaging spectrometer and telescope system designed for integration on a 6U CubeSat platform. Operating in the 350-1700 nm spectral region with 5.7 nm sampling, SWIS is capable of simultaneously addressing the demanding needs of coastal ocean science and snow/ice monitoring. We discuss progress in the SWIS optomechanical design, thermal analysis, and mission plan. We also describe an innovative single drive on-board calibration system capable of addressing the stringent radiometric stability and knowledge these missions require. The spectrometer features a new Teledyne CHROMA array, optimized for high temperature operation, with a linear variable anti-reflection coating to enhance quantum efficiency and minimize backscatter.

**Keywords:** imaging spectroscopy, Dyson spectrometer, CubeSat, snow cover, coastal ocean

## 1. INTRODUCTION

Imaging spectroscopy places heavy demands on a satellite, in terms of aperture size, data volume, and power. To stay within CubeSat resources, certain adaptations are required. Size and power constraints dictate a limited spatial resolution, and the avoidance of cryogenic temperatures limits the wavelength range. Low data volume and rates place further restrictions on potential targets. Given these constraints, there exist critical niche applications with localized areas of interest that have the potential to be well-served with a CubeSat platform. We explore two such regions: coastal ocean zones, and snow or ice covered mountains.

The requirements for a coastal ocean spectrometer have been discussed in Ref. 1 and include high throughput for sufficient signal from the low-reflectivity water surface, fast readout rate for high dynamic range, and low polarization. The high spatial variability of coastal targets requires higher resolution than heritage sensors, which typically have greater than 500 m resolution. Such resolution is adequate for global ocean science, but is too coarse for studying coastal areas. The Portable Remote Imaging Spectrometer (PRISM) is an airborne sensor that has been shown to meet the requirements for coastal ocean imaging.<sup>2</sup> However, the high temporal variability in many regions of interest potentially requires consistent airborne monitoring, which becomes costly.

While coastal ocean spectral signatures exist mainly below 0.9  $\mu\text{m}$ , extending our spectral range allows us also to map snow and ice spectral signatures, which contain critical features into the near-infrared and shortwave-infrared. In the visible spectrum, snow reflectance is degraded by contaminants such as dust and black carbon. As snow grain size increases, we observe reduced reflectance in wavelengths beyond 0.8  $\mu\text{m}$ .<sup>3</sup> An imaging spectrometer with high spatial and temporal resolution can measure the changes in albedo caused by snow grain size, dust deposition and black carbon. These albedo measurements help us understand the loss of snow and ice mass, which has consequences for the climate, sea level rise, and the availability of water resources.

---

Corresponding author: \*[holly.a.bender@jpl.nasa.gov](mailto:holly.a.bender@jpl.nasa.gov); Address: Jet Propulsion Laboratory, 4800 Oak Grove Drive, MS 306-392, Pasadena, CA, USA 91109.

The Snow and Water Imaging Spectrometer (SWIS) is particularly well-suited to address critical science in these two localized regions of the Earth. It is designed to operate over a range of 350-1700 nm, covering both coastal ocean and snow/ice spectral regions of interest, with 5.7 nm spectral sampling. The telescope and spectrometer operate at F/1.8. At 100 mm focal length, the telescope provides 160 m resolution from an orbit of 500 km and is the highest resolution form able to fit in the 6U CubeSat frame (approximately 10 cm x 20 cm x 30cm) without deployable mirrors. The field of view is 10° with 600 cross-track pixels. Pointing capability of  $\pm 20^\circ$  provides a 50° field of regard.

Fig. 1 shows a conceptualized image of the SWIS 6U CubeSat spacecraft, along with one possible mission configuration emphasizing high temporal resolution. Using six SWIS CubeSat spacecraft (each with a 50° field of regard) evenly spaced at a 500 km orbit, we achieve the flexibility to access any point on the globe at least once on a given day.

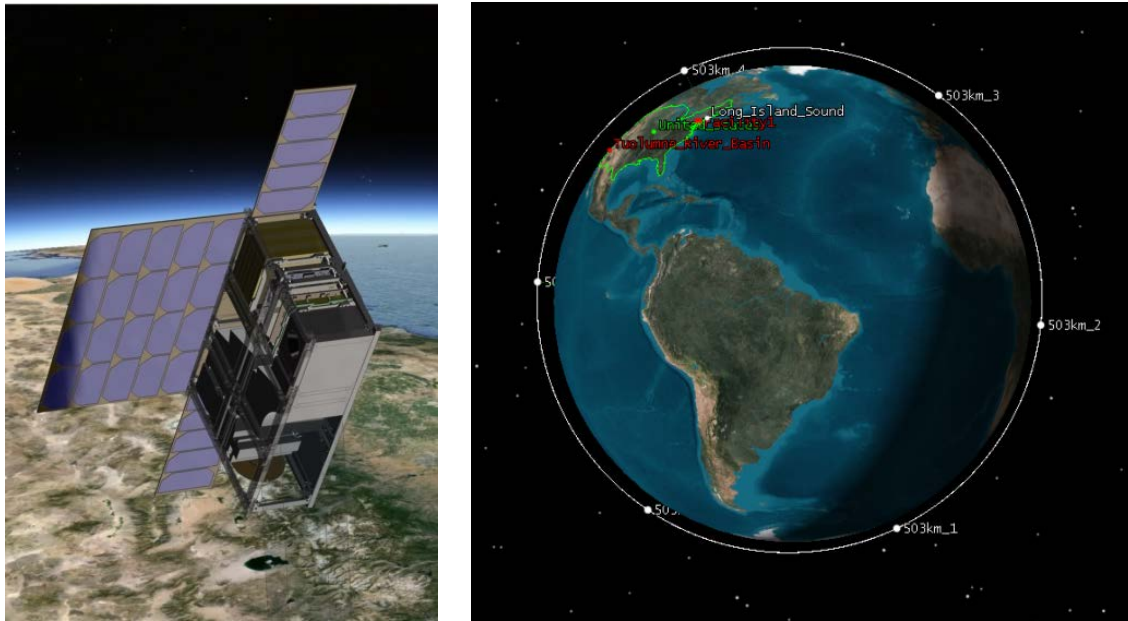


Fig 1: *Left*: An artist's concept of the SWIS 6U CubeSat spacecraft, the spectrometer and telescope contained within the lower 4U; *Right*: One example of several possible configurations places 6 SWIS CubeSats evenly spaced at a 500 km orbit, each with a 50° field of regard, for flexibility to access any point on the globe on a given day.

The SWIS instrument benefits from a rich heritage of imaging spectrometer development at the Jet Propulsion Lab (JPL), including the Portable Remote Imaging Spectrometer (PRISM),<sup>2</sup> Ultra-Compact Imaging Spectrometer (UCIS),<sup>4</sup> Next-Generation Imaging Spectrometers (NGIS),<sup>5</sup> Moon Mineralogy Mapper (M<sup>3</sup>),<sup>6</sup> and Mapping Reflected-energy Sensor (MaRS)<sup>7</sup> instruments. A critical component of the design is the diffraction grating, made at JPL, which has a tailored broadband response and low polarization sensitivity. New key technologies that facilitate the development of this instrument include a linear variable anti-reflection (LVAR) detector coating for stray light management, and a single drive on-board calibration mechanism utilizing a transmissive diffuser for solar calibration.

## 2. SNOW AND WATER IMAGING SPECTROMETER (SWIS) DESIGN

### 2.1 Optical design and specifications

The SWIS instrument consists of a three-mirror anastigmat (TMA) telescope and Dyson form spectrometer. Details of the optical design and system performance have been described previously in Ref. 8. A system raytrace is shown in Fig. 2, overlaid with a 20 cm x 30 cm rectangle representing the footprint of a 6U frame (depth is 10 cm). The spectrometer and telescope are well contained within 4U of the available area.

System specifications are shown in Table 1. In order to meet the standards of high performance imaging spectroscopy, typical desired non-uniformity values are < 5% of a pixel for geometric non-uniformities, and < 10% for full width at half-maximum variation.<sup>10,11</sup> While there are various post-processing techniques for smile and keystone through resampling,<sup>12</sup> minimizing these errors avoids unnecessarily complex data reduction processes. SWIS smile and keystone are negligible at less than 1% of a 30  $\mu\text{m}$  pixel, with expected response function FWHM variation at 10% or better.<sup>8</sup>

Table 1: SWIS system specifications

Property	Value
Spectral range	350-1700 nm
Spectral sampling	5.7 nm (/30 $\mu\text{m}$ )
Cross track spatial elements	600 (+40 monitor)
Uniformity	95%
Resolution	0.3 mrad
Slit width	30 $\mu\text{m}$
Working F-number	1.8
Cross track FOV	10° ( $\pm 20^\circ$ pointing)

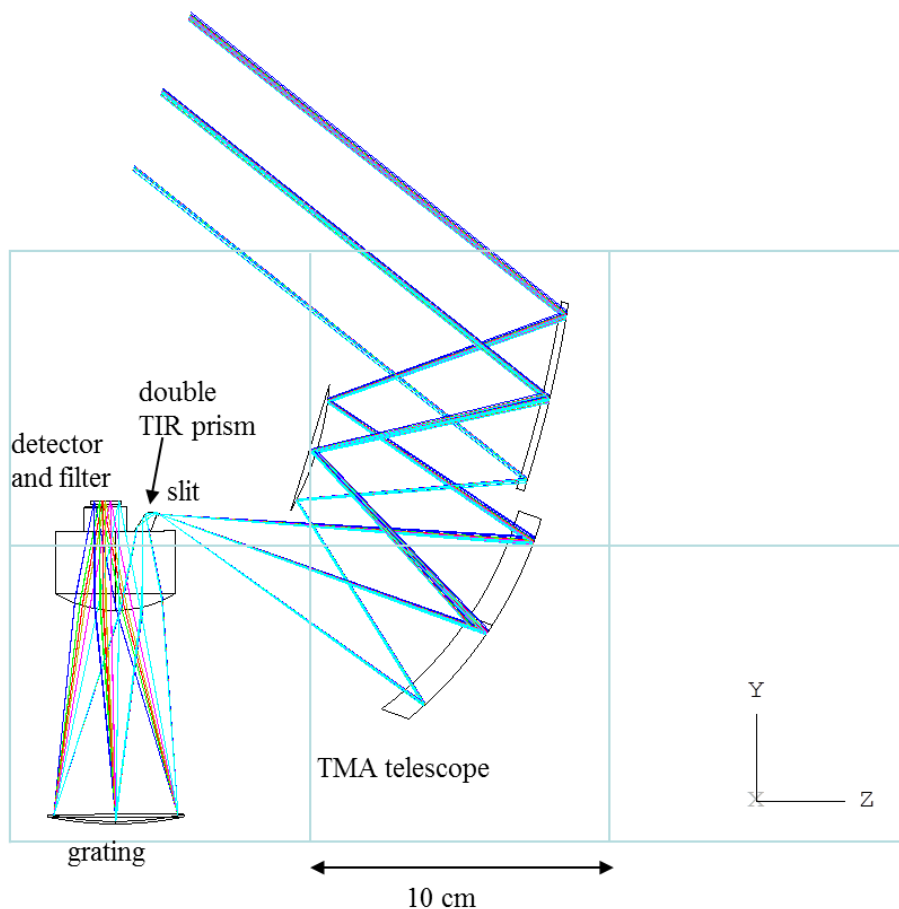


Figure 2: Spectrometer and telescope raytrace overlaid with a 20 cm x 30 cm rectangular footprint, approximating a 6U CubeSat frame. The frame extends 10 cm in the x-direction, and telescope mirror size is maximized within that available space. The folding arrangement is made possible by a small prism used in dual total internal reflection.

## 2.2 Stray light

Stray light is a significant concern and driver of the design. A stray light analysis for this instrument is presented in Ref. 8, along with steps taken to mitigate its effects. These include judicious positioning of the slit,<sup>2</sup> optimization of dispersion to exclude zero order reflected ghosts, and ensuring that all reflected ghosts are returned in negative (weak) grating orders. While ghost location and intensity can be partially controlled through these first order system parameters, stray light control ultimately depends critically on the properties of the detector anti-reflection coating and the order-sorting filter. To this end, we are working with Teledyne Scientific & Imaging in the development of a linear variable anti-reflection (LVAR) coating. Measured data from Teledyne with this new coating technology (Fig. 4) shows reflectivity of <1% for 350 to 1700 nm, with nearly all wavelengths having <0.5% reflectivity.

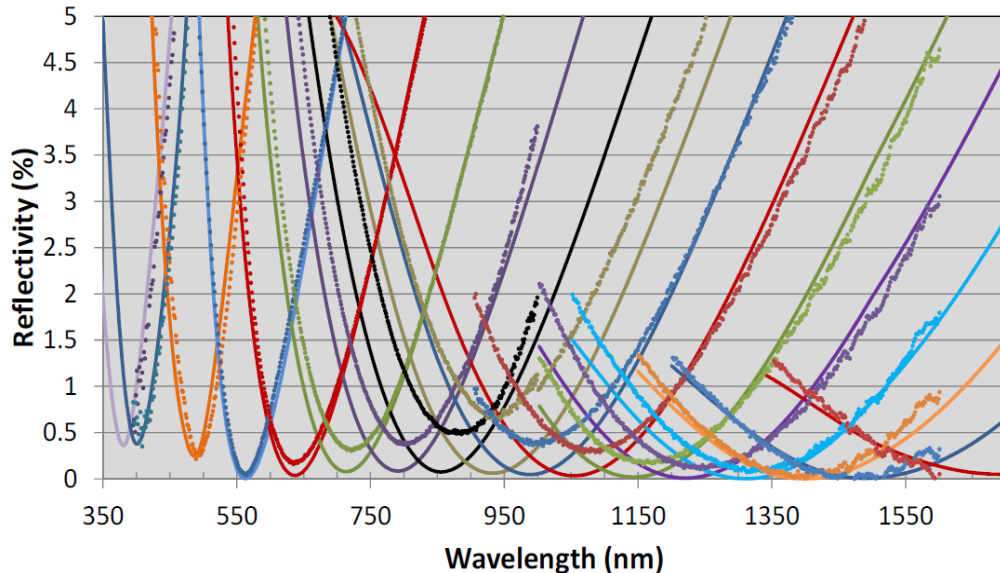


Figure 4: Measured data of the linear variable anti-reflection (LVAR) detector coating under development at Teledyne Scientific & Imaging shows <1% reflectivity for 350-1700 nm, with nearly all wavelengths having <0.5% reflectivity

## 2.3 Optomechanical Design

The SWIS optomechanical system (Fig. 5) is designed to meet tight optical alignment accuracy and stability requirements, with size constrained for the CubeSat environment, and at a lower cost than is typically found in prior spaceflight and airborne payloads. Our design approach involves employing the stable and high-resolution mounts proven on many of the aforementioned heritage JPL sensors<sup>2,4-6</sup> while utilizing common materials and standard machining throughout. To further keep down cost, rapid prototyping techniques are used where appropriate, ie: on complex shapes with low mechanical stress and non-critical tolerances. Interfaces between mounts, elements, and components are designed to avoid hysteresis.

The optomechanical assembly fits within 4U (10 cm x 20 cm x 20 cm) of the 6U CubeSat frame (Fig. 5). Total combined mass of the optomechanical assembly is 1.84 kg, with 967 g attributed to the telescope, 679 g from the spectrometer, and 195 g for instrument interface bipods and fittings.

The telescope housing is designed for ease of machining and assembly, and given the benign operating temperature and narrow range, is made from aluminum. Mirror mount flexures are separate from the housing and made of titanium alloy to minimize fabrication risk and to buffer the thermal expansion differential between the aluminum housing and the optical glass mirror substrates. Mirrors are bonded to the mirror mounts with CV2566 silicone adhesive. Bipods with flexured end-fittings provide thermal and structural isolation between the telescope housing and the CubeSat frame.

The spectrometer assembly leverages airborne Dyson spectrometer designs,<sup>2,4</sup> and incorporates a six degree of freedom focal plane mount (Fig. 6) that has been tested and proven capable of sub-micron accuracy. The grating mount (Fig. 7) also relies on heritage designs, but with enhancements for added stability. The grating mount features three flexure supported bond pads and a clocking adjustment tangent rod for arc-second resolution and stable clocking control. The mount succeeds in adequately decoupling clocking adjustment and unwanted decentration, as shown in Fig. 8. As in the telescope, the grating optic is bonded to the mount using CV2566 adhesive. Although the spectrometer is expected to operate at a nominal 290 K, a finite element model of the grating, adhesive, and mount was generated for  $\Delta T = 60$  K, and showed negligible effect on the grating substrate figure, as shown in Fig. 9.

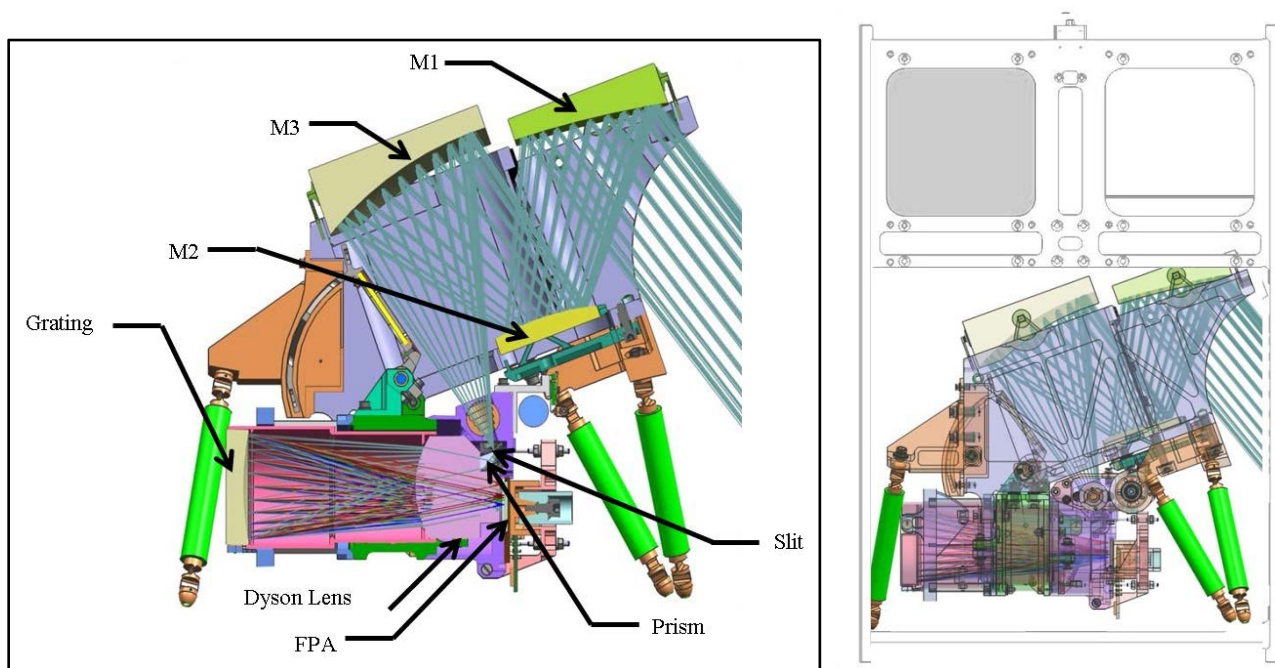


Figure 5: *Left*: SWIS optomechanical model section view showing optical elements; *Right*: Orientation in 6U CubeSat frame

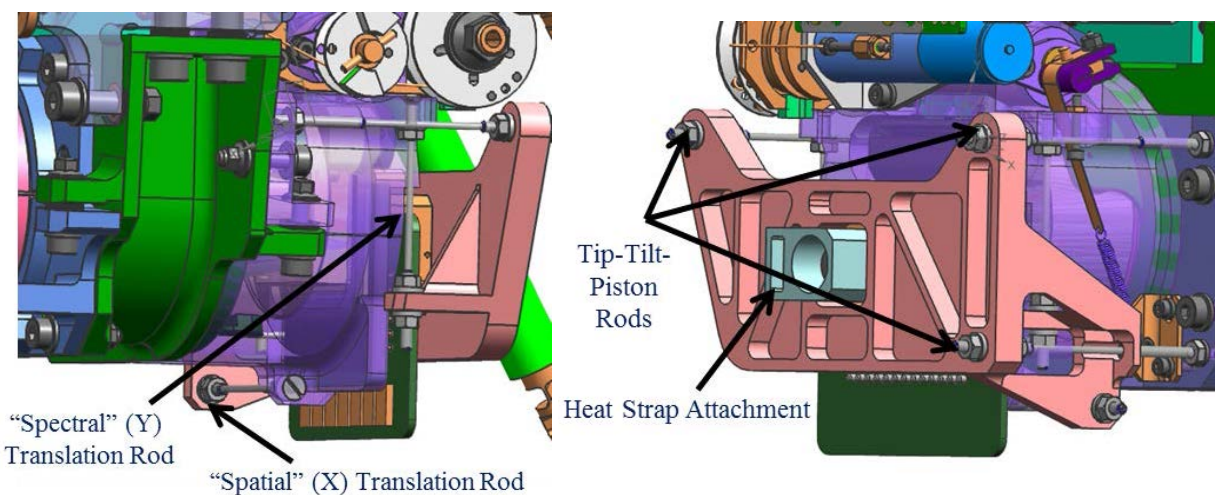


Figure 6: Focal plane array mount has 6 degrees of freedom and is capable of sub-micron resolution.

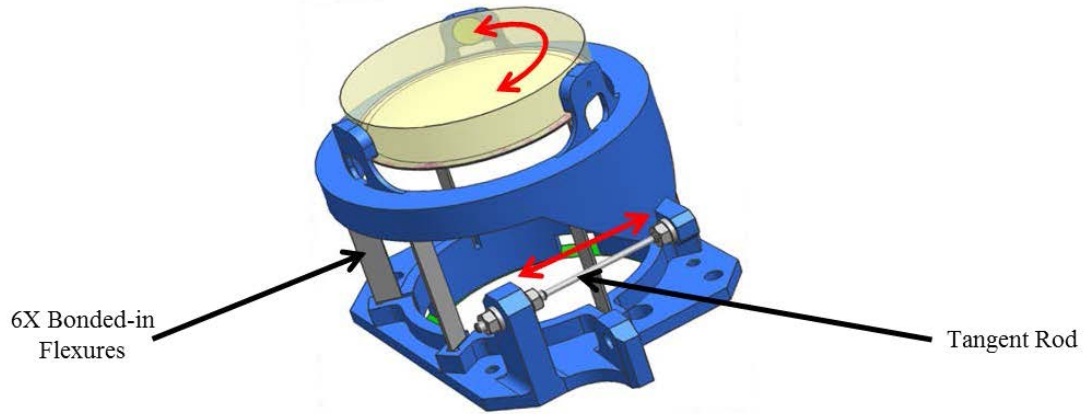


Figure 7: Grating mount with clocking adjustment tangent rod for arc-sec resolution and stable clocking control

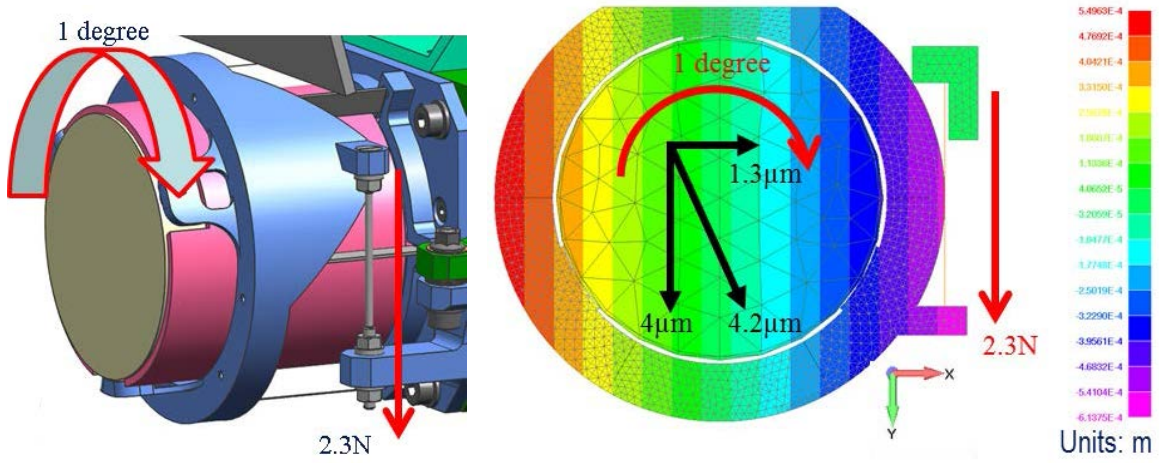


Figure 8: *Left:* Grating mount analysis demonstrates coupled decentration with 1 deg of rotation adjustment (2.3 Newtons force on the clocking rod). *Right:* The resulting combined translation is 4.2  $\mu\text{m}$ , easily tolerable during the alignment stage when the rod is used.

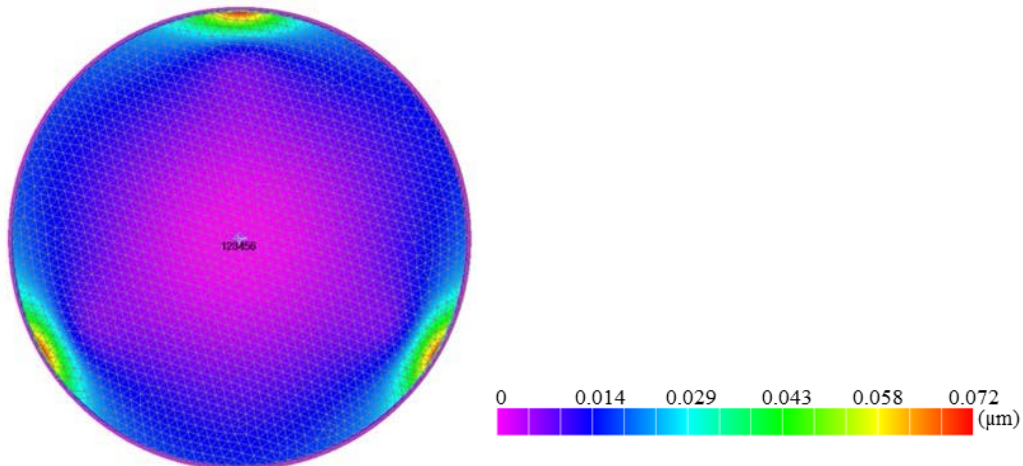


Figure 9: Finite element model of the grating shows a peak-to-valley surface deformation of  $0.11\lambda$  for  $\Delta T = 60 \text{ K}$ .

## 2.4 Calibration mechanism and diffuser testing

For an imaging spectrometer, the quality of the data and the ability to complete a science grade mission depends on the calibration strategy. Specifically, we require a spectral calibration accuracy approaching 1% of the full width at half-maximum throughput of the spectral response function.<sup>13</sup> With the SWIS instrument, we demonstrate a calibration system capable of addressing the stringent radiometric stability and knowledge needed to serve its science mission. We accomplish this with a new single drive mechanism (Fig. 9, 10) that performs the dual function of positioning the on-board calibrator (OBC) as well as providing a shutter for dark frames.

The diffuser material selected for solar calibration is Heraeus OM-100, which is Lambertian enough that we might achieve stable illumination without the need for highly accurate CubeSat pointing (Fig. 11). A testbed simulating the collection geometry of the spectrometer and the sun is shown in Fig. 12. Test results indicate the Heraeus OM-100 diffuser, when oriented as in the CubeSat configuration, has an expected radiance equivalent to a surface with a reflectance of 10 to 13%. This satisfies our requirements for imaging spectroscopy calibration. The specific diffuser to be used in an eventual flight instrument will be characterized to an accuracy of 1% or better.

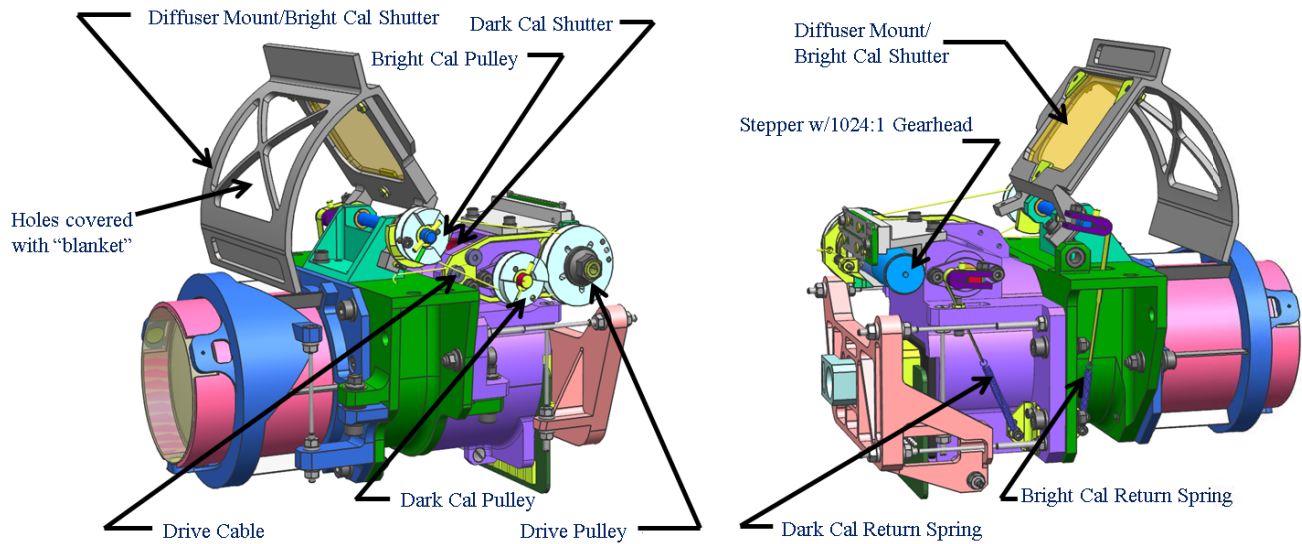


Figure 9: Calibration mechanism performs dual function of positioning the on-board calibrator (OBC) as well as providing a shutter for dark frames, is shown in the open (“science”) position

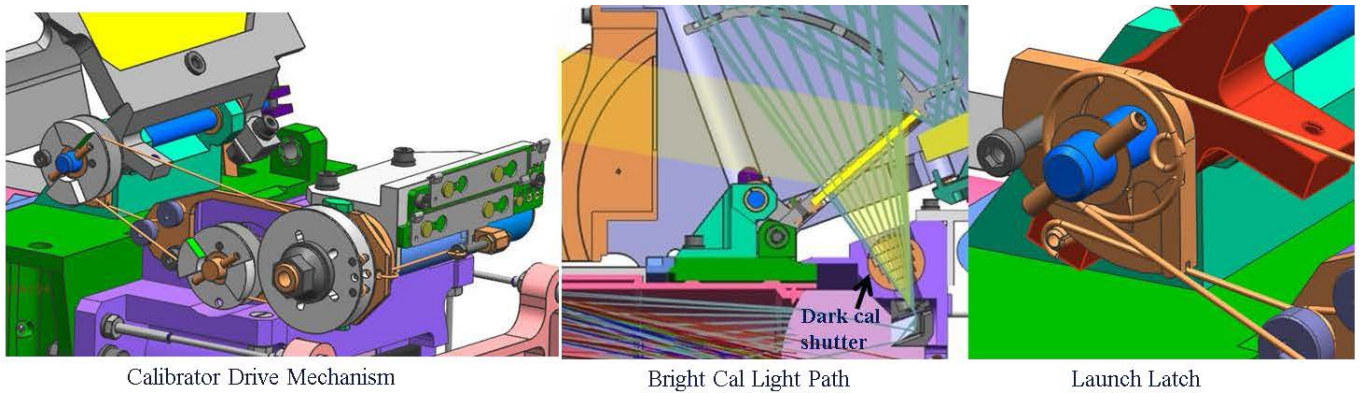


Figure 10: A Dyneema drive cable operates in tension against a return spring (*left*), actuating bright and dark calibrators. In the solar calibration position (*center*), the diffuser mount blocks signal from the telescope. A dark calibration shutter rotates to a closed position for darks. The mechanism also includes a launch latch (*right*) released on first usage, and a fail-safe.

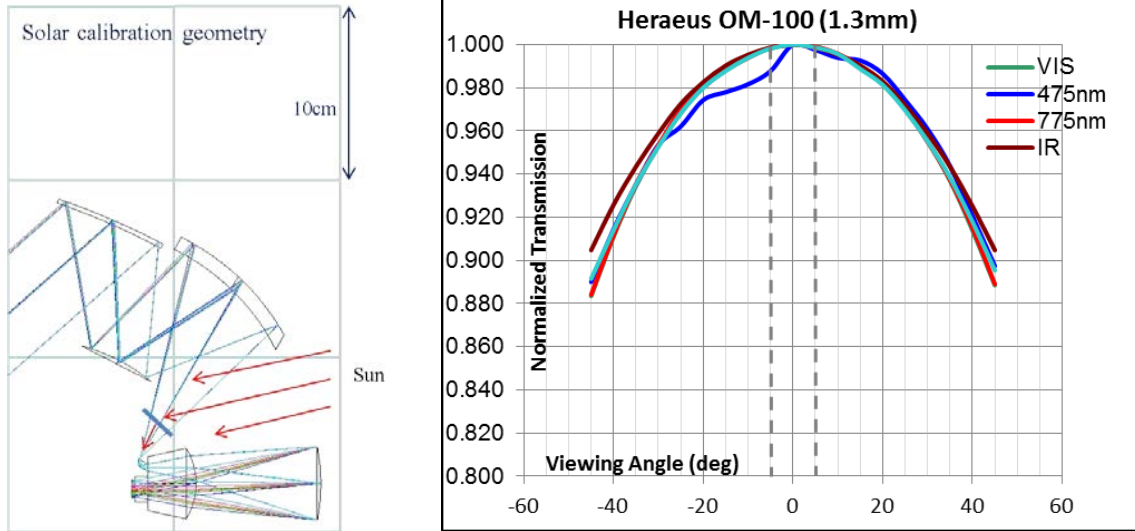


Figure 11: *Left*: Spectrometer and telescope in 6U-sized frame shows solar calibration geometry; *Right*: Diffuser material Heraeus OM-100 demonstrates near uniform transmission within  $\pm 5^\circ$ , thus highly accurate CubeSat pointing is not necessary for stable illumination.

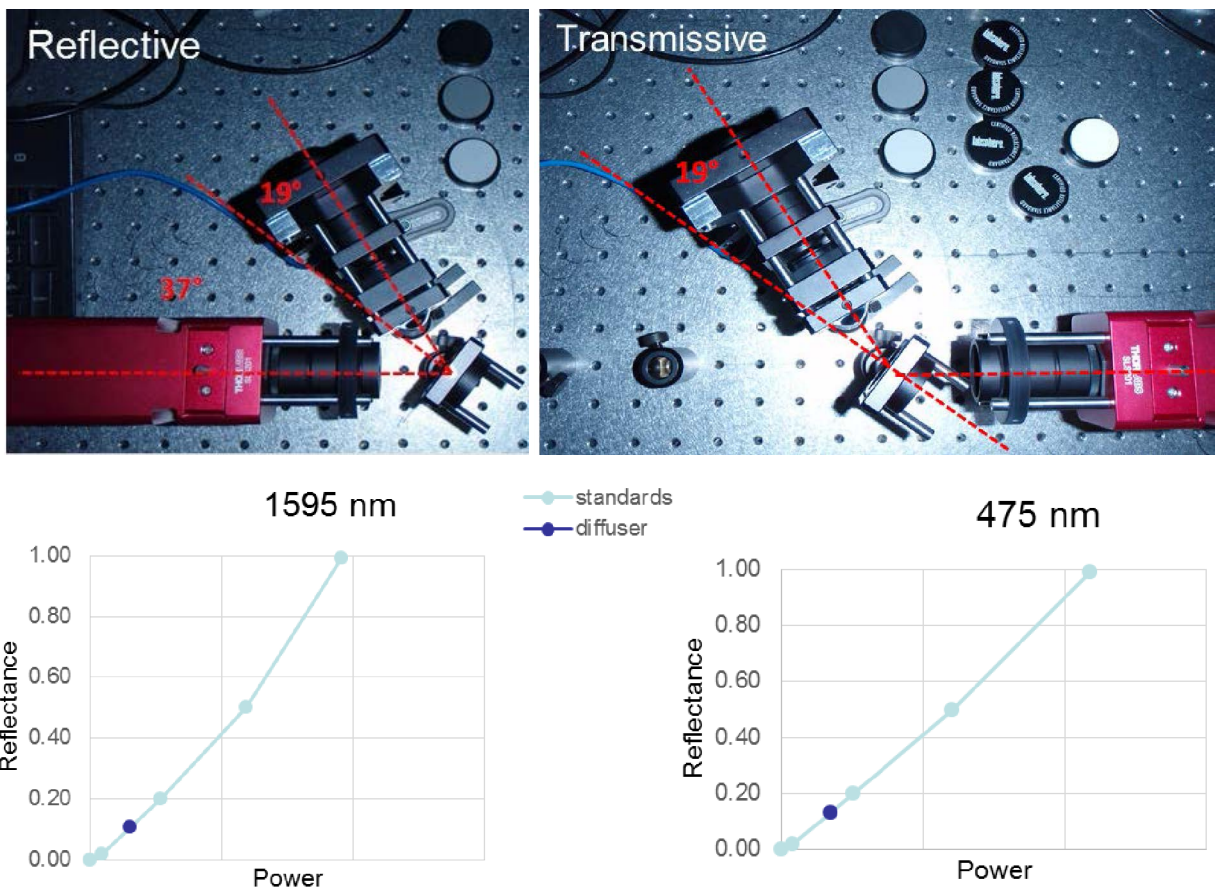


Figure 12: *Top*: Diffuser material testing setup simulates the solar collection geometry of the spectrometer in reflective (*left*) and transmissive (*right*) configurations; *Bottom*: The Heraeus OM-100 diffuser oriented as in the CubeSat configuration has an expected radiance equivalent to a surface with a reflectance of 10% (*left*) to 13% (*right*), dependent upon wavelength.

## 2.5 Thermal design

SWIS has three important thermal requirements. The first requirement is to maintain all components within their operational and non-operational temperature limits. Most components have unremarkable temperature limits, but the focal plane array (FPA) must be held below 250 K, which implies nontrivial thermal design. In addition there are two notable stability requirements: the FPA temperature must be stable to  $\pm 0.1$  K, and the spectrometer temperature must be stable to  $\pm 1$  K.

The top-level thermal architecture is shown in Fig. 11. To move heat through the structure and into space, the bus electronics and FPA electronics are mechanically and thermally well-connected to the spacecraft. The FPA, which has a tight stability requirement, is thermally isolated from the spacecraft, which varies in temperature significantly over the orbit. This thermal isolation alone keeps the FPA temperature variation less than 2.5 K. To control the temperature to  $\pm 0.1$  K, a 1.5 W heater in a PID control loop is added to the FPA support structure. Since the FPA must be stable but also relatively cold, the FPA support structure is thermally linked to a dedicated radiator, which is mounted on the side of the spacecraft with no direct view of the sun throughout the orbit. Radiation shields are used to reduce heat transfer between the structure and the cooler, and the cooler is mounted to the spacecraft on low-conductivity spacers. A 1 W heater is added to the optics to keep the temperature above the operational limit.

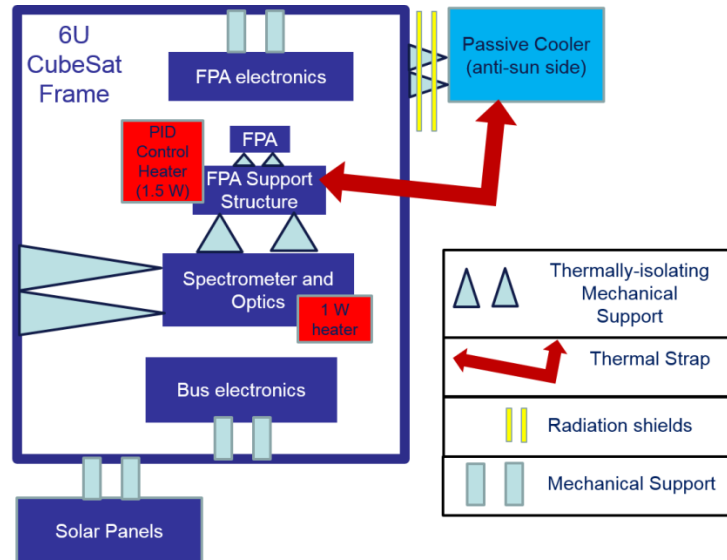


Figure 11: The top-level thermal architecture is described by the following major components: the focal plane (FPA), focal plane support, spectrometer and optics, FPA electronics, bus electronics, solar panels, CubeSat frame and passive cooler

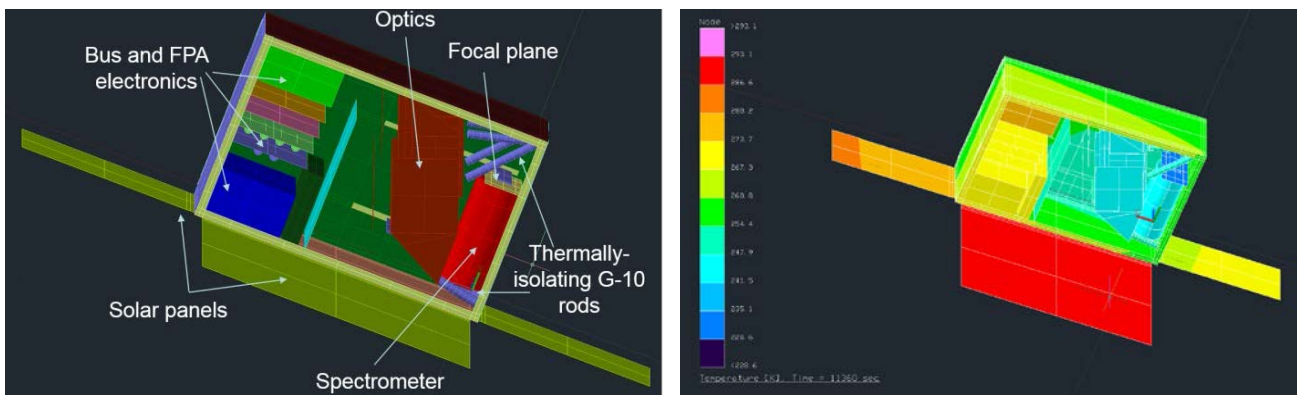


Figure 12: Image of Thermal Desktop Model (left), with representative temperature data (right) simulating orbit environment and conductive and radiative heat transfer.

A Thermal Desktop Model (Fig. 12) was built with geometric similarity to the present spacecraft design. The power dissipation in the spacecraft was estimated based on laboratory testing for the focal plane electronics, past and current CubeSat missions at the Jet Propulsion Laboratory, and datasheets for commercial parts. Fig. 13 shows the temperature as a function of time for the focal plane and the spectrometer under a nominal condition (beta angle = 37 degrees, altitude = 500 km). These data indicate that the requirements are met for the mean temperature and thermal stability of the focal plane and the spectrometer. Other data indicate the rest of the spacecraft components have on-orbit temperatures within the component temperature limits.

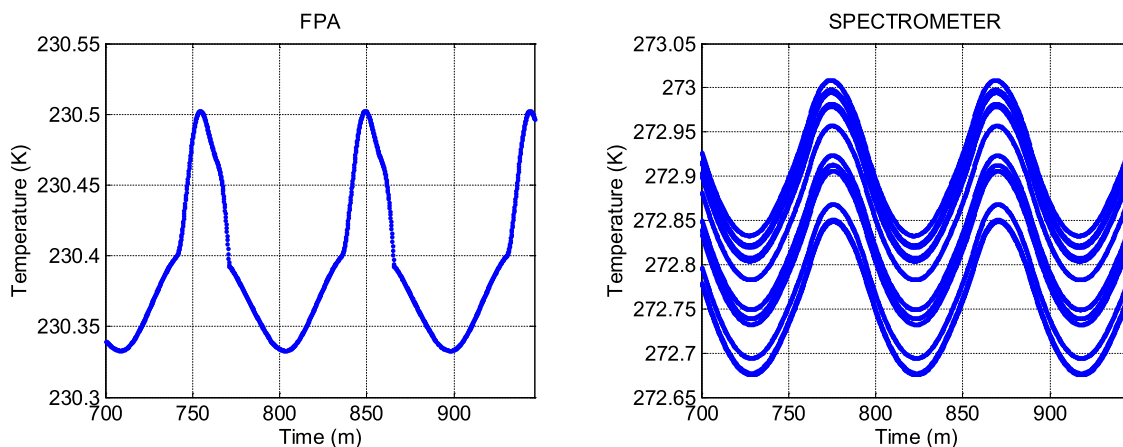


Figure 13: Model predictions of FPA (left) and spectrometer (right) temperatures show mean and stability requirements are met

## 2.6 Spacecraft configuration

The current spacecraft configuration (Fig. 14) is favorable for accommodation in a 6U CubeSat frame. Components have been identified and designed specifically to fit within a 6U Canisterized Satellite Dispenser available from Planetary Systems Corporation.

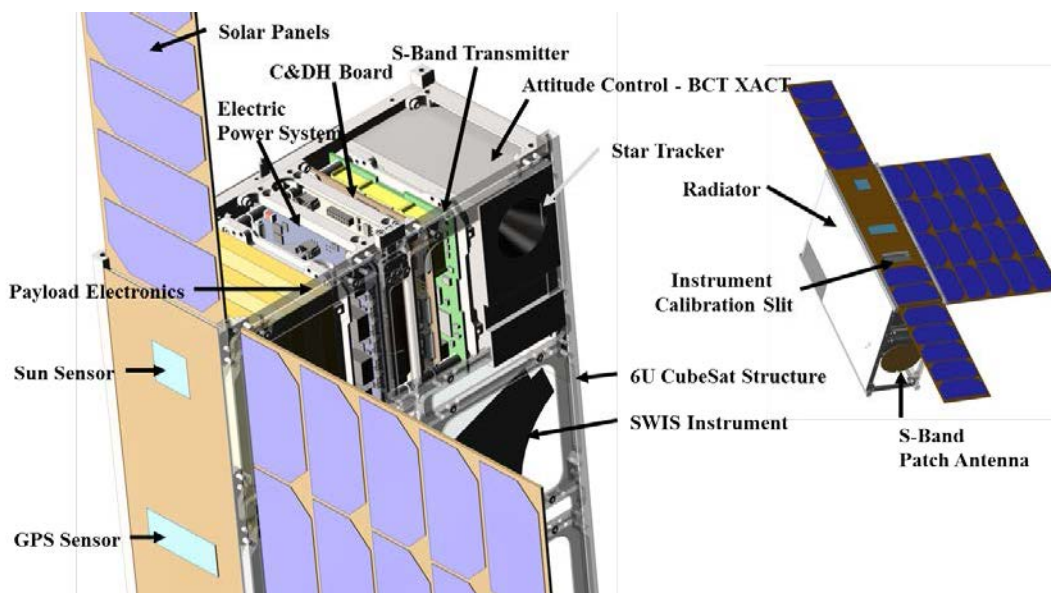


Figure 14: SWIS CubeSat configuration within a 6U structure

### 3. CONCLUSIONS

We present a high-heritage, science-grade imaging spectrometer design suitable for CubeSat applications. The design advances the state of the art in compact sensors of this kind in terms of size and spectral coverage. New enabling technologies include a linear variable anti-reflection (LVAR) coating to provide a critical reduction in stray light, and a single drive on-board calibrator (OBC) for solar and dark calibration. The current spacecraft configuration is well-contained within a standard commercial 6U frame. Useful missions can be designed using the SWIS instrument to address targeted areas of the Earth's surface with high spatial and temporal resolution, and high throughput signal to noise. Potential science applications have been identified as coastal ocean and snow/ice covered mountain regions.

### ACKNOWLEDGMENTS

The research in this paper was performed at the Jet Propulsion Laboratory, California Institute of Technology under contract with the National Aeronautics and Space Administration. Reference herein to any specific commercial product, process, or service by trade name, trademark, manufacturer, or otherwise, does not constitute or imply its endorsement by the United States Government or the Jet Propulsion Laboratory, California Institute of Technology. Development of the linear variable anti-reflection (LVAR) coating is in collaboration with Teledyne Scientific & Imaging under the leadership of Dr. Jianmei Pan. We thank Daniel Preston and Glenn Sellar for their assistance in obtaining diffuser material measurements, and the rest of the SWIS team: Ernesto Diaz, Thomas Painter, Heidi Dierssen, Paula Pingree, Elliott Liggett, and Robert Green for their contributions.

### REFERENCES

- [1] Mouroulis, P., Green, R. O., Wilson, D. W., "Optical design of a coastal ocean imaging spectrometer," *Opt. Express* 16, 9087-9095 (2008).
- [2] Mouroulis, P. et al, "Portable Remote Imaging Spectrometer coastal ocean sensor: design, characteristics, and first flight results," *Appl. Opt.* 53(7), 1363-1380 (2014).
- [3] Dozier, J., Green, R. O., Nolin, A. W., Painter, T. H., "Interpretation of snow properties from imaging spectrometry," *Remote Sensing of Environment*, 113, 525-537 (2009).
- [4] Van Gorp, B. et al, "Optical design and performance of the Ultra-Compact Imaging Spectrometer (UCIS)," *Imaging Spectrometry XVI, Proc. SPIE*, 8158, 81580L (2011).
- [5] Bender, H. A., Mouroulis, P., Green, R. O., Wilson, D. W., "Optical design, performance and tolerancing of next-generation airborne imaging spectrometers," *Imaging Spectrometry XV, Proc. SPIE*, 7812, 78120P (2010).
- [6] Green, R. O., et al., "The Moon Mineralogy Mapper (M3) imaging spectrometer for lunar science: Instrument description, calibration, on-orbit measurements, science data calibration and on-orbit validation," *J. Geophys. Res.* 116, E00G19 (2011).
- [7] Simi, C., Reith, E., Olchowski, F., "The Mapping Reflected-energy Sensor - MaRS: A New Level of Hyperspectral Technology," *Proc. SPIE* 7457, 745703 (2009).
- [8] Mouroulis, P, Van Gorp, B., Green, R. O., Wilson, D. W., "Optical design of a CubeSat-compatible imaging spectrometer," *Imaging Spectrometry XIX, Proc. SPIE*, 9222, 92220D (2014).
- [9] Green, R. O., "Spectral calibration requirement for Earth-looking imaging spectrometers in the solar-reflected spectrum," *Appl. Opt.* 37, 683-690 (1998).
- [10] Mouroulis, P., Sellar, R. G., Wilson, D. W., Shea, J. J., and Green, R. O., "Optical design of a compact imaging spectrometer for planetary mineralogy," *Opt. Eng.*, 46(6), 063001 (2007).
- [11] Bender, H. A. et al, "Alignment and characterization of high uniformity imaging spectrometers," *Imaging Spectrometry XVI, Proc. SPIE*, 8158, 81580J (2011).
- [12] Neville, R. A., Sun, L., Staenz, K "Detection of spectral line curvature in imaging spectrometer data," *Algorithms and Technologies for Multispectral, Proc. SPIE*, 5093, 144-154 (2003).
- [13] Green, R. O., "Spectral calibration requirement for Earth-looking imaging spectrometers in the solar-reflected spectrum," *Appl. Opt.* 37, 683-690 (1998).